VERIZONA PUBLISHER
Publishing Your Ideas

www.verizonaonlinepublishing.com
Vol: 1, Issue: 1

Journal of Applied and Theoretical Physics Research

Structure and Spectroscopy of *o*-anisidine Investigated by Density Functional Theory in Comparison with Experiments

Ahmet Altun[1,2,*] **and Kubra Fevzioglu**[1]

[1]Department of Physics, Fatih University, Büyükçekmece, Istanbul 34500, Turkey

[2]Department of Genetics and Bioengineering, Fatih University, Büyükçekmece, Istanbul 34500, Turkey

***Corresponding author:** Ahmet Altun, Department of Physics, Fatih University, Büyükçekmece, Istanbul 34500, Turkey; Tel: +90-212-866-3300; Fax: +90-212-866-3402; Email: aaltun@fatih.edu.tr

Article Type: Research, **Submission Date**: 13 November 2015, **Accepted Date:** 01 December 2015, **Published Date:** 07 January 2016.

Citation: Ahmet Altun and Kubra Fevzioglu (2016) Structure and Spectroscopy of o-anisidine Investigated by Density Functional Theory in Comparison with Experiments. JApl Theol 1(1): 1-13.

Abstract

The molecular structures, vibrational spectra (IR and Raman), UV-Vis electronic absorption spectra, and NMR spectra (^{13}C and ^{1}H) of *o*-anisidine have been investigated in terms of density functional theory by using B3LYP as a density functional and 6-311++G** as a basis set. Two stable and virtually degenerate conformers arising from non-planarity of the amino group of *o*-anisidine have been located at the room temperature. All normal modes of *o*-anisidine have been assigned in terms of percent contributions of the internal motions. All main electronic transitions in the UV-Vis spectrum of *o*-anisidine have been assigned. Solution that increases ionization potential of *o*-anisidine but decreases its electron affinity has been shown to affect the unoccupied orbitals of *o*-anisidine drastically, which shift all electronic absorption bands to longer wavelengths. The frontier molecular orbital, molecular electrostatic potential map, and atomic charge (Mulliken, ESP, and NBO) analyses have been shown useful in estimating both global and atom-in-molecule characteristics of *o*-anisidine. The present chemical shift calculations allow certain assignments of the experimental ^{13}C and ^{1}H NMR signals of *o*-anisidine. The high correlations between the experimental and the present computational spectral data indicate that the computational route presented in this study can be extended for the spectroscopic calculations of analogous compounds.

Keywords: Aniline derivatives, Density Functional Theory (DFT), Infrared, Raman, UV-Vis, NMR.

Introduction

Aromatic amines like aniline and its derivatives have enormous applications in chemical, biological, pharmaceutical, and materials sciences and industries. Spectroscopic characterization of aniline derivatives in both ground and excited states attract considerable attention to better understand their molecular properties and chemical reactions [1-10].

o-Anisidine (known also as 2-methoxyaniline) is a methoxy ($-OCH_3$) derivative of aniline at the *ortho* position (Figure 1). Although many pigments and dyes that are widely used in printing, and paper and textile dyeing are manufactured using *o*-anisidine, it is an industrial and environmental pollutant causing tumors of the urinary bladder in rats and mice, with potent carcinogenicity to human. In addition to its release from textiles and leather products, cigarette smoke releases also this carcinogen. *o*-Anisidine exhibits many other toxic effects, including hematological changes, anemia, and nephrotoxicity. It is also mutagenic to *Salmonella*. Hepatic microsomal cytochrome P450 enzymes in human, rat, and rabbit play an important role in the detoxification of this carcinogen [11-14].

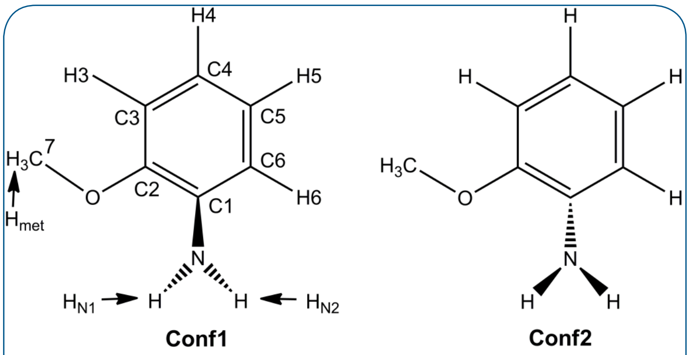

Figure 1: Two possible conformations of *o*-anisidine and the atom labeling scheme

Spectroscopic measurements offer an opportunity for the identification of toxic compounds in industrial processes and products so that such hazardous processes cannot be used anymore in manufacturing and such toxic products can be withdrawn from the markets. Many spectroscopic measurements were performed on *o*-anisidine [15-18]. However, the characteristics of these recorded spectra were not analyzed despite their importance in controlling safety of the manufacturing processes and the resulting industrial products.

Density functional theory (DFT) calculations with hybrid functionals like B3LYP [19,20] are known to give quite accurate results for the geometrical and spectral characteristics of molecular systems. In this study, we investigate structural and spectral characteristics of *o*-anisidine with the B3LYP functional, In particular, conformational stabilities, key geometry parameters, charge distribution and electrostatic potential analyses, vibrational spectra (both IR and Raman), UV-Vis electronic absorption spectra with frontier orbital analyses, and ^{1}H and ^{13}C nuclear magnetic resonance spectra of *o*-anisidine has been investigated.

Computational details

All quantum chemical calculations were performed by using Gaussian 03 program package [21]. The geometrical structures of all possible conformers of *o*-anisidine were optimized by using the hybrid B3LYP [19,20] density functional with the double-ζ 6-31G* and the larger triple-ζ 6-311++G** split-valence basis sets [22-24]. Unless stated otherwise, these molecular characteristics were calculated at the B3LYP/6-311++G** level. In some certain cases, the effects of the use of the 6-31G* basis set were examined.

Force fields of the compounds were calculated in the space of Cartesian coordinates by analytic differentiation. They were then transformed to internal coordinates for assigning normal modes in terms of internal motions (stretching ν; out-of-plane deformation γ; in-plane deformation β) with their percent contributions to the potential energy distribution (PED).

B3LYP overestimates vibrational frequencies systematically as a result of the neglect of the effects of environment and anharmonicity, and the incompleteness of basis set and dynamical correlation. Thus, the calculated frequencies are mostly scaled for relating the computed and experimental frequencies [25,26]. We derived the scaling factors that are the correlation coefficients between the experimental and computed frequencies on benzene. The structure and vibrational spectra of benzene were determined again at the B3LYP/6-311++G** level. The scaling factors were found on benzene as 0.964 (R^2= 0.64) for the frequencies above 2800 cm^{-1}, which correspond to X–H stretchings (X = C, N, S, etc.), and as 0.981 (R^2 = 1.00) for the frequencies below 2800 cm^{-1}.The R^2 value of the correlation for the frequencies below 2800 cm^{-1} is 1.00, which indicates that the found factor can be used in scaling computational frequencies of the related molecules. However, it is 0.64 for the frequencies above 2800 cm^{-1}, analogous to those obtained on other related compounds [27,28]. Thus, the present scaling factor for the X-H stretchings may not be accurate enough for other compounds. The largeness of the deviations between the experimental and the scaled X-H stretching frequencies can be attributed to their strong anharmonicities and local environment differences, i.e., vacuum (calculation) vs. liquid (experiment). The simulated IR and Raman spectra of *o*-anisidine were obtained using computational frequencies (ν_i) scaled with the two factors found on benzene (0.964 and 0.981), computed IR intensities ($I_{IR,i}$), and Raman intensities ($I_{Ra,i}$) found through the computed Raman activity ($S_{Ra,i}$) using the following equation derived from Raman scattering theory for each mode *i* [29-31]:

$$I_{Ra,i} = \frac{f(\nu_0 - \nu_i)^4 S_{Ra,i}}{\nu_i \left[1 - \exp(-\frac{hc\nu_i}{kT}) \right]}$$

where *h*, *c*, and *k* are Planck's constant, speed of light, and Boltzmann's constant; *f* is a factor that is common for all peak intensities; ν_0 is the excitation line of the laser used in Raman measurements in cm^{-1}, i.e., 9398.5 cm^{-1} corresponding to 1064 nm line of the near infrared Nd:YAG air-cooled laser. IR and Raman spectra were simulated by using pure Lorentzian band shapes taking the full widths at the half-height (FWHH) as 10 cm^{-1}.

UV-Vis electronic absorption spectra were calculated with time-dependent (TD)-DFT method utilizing B3LYP functional and 6-311++G** basis set in both gas phase and in ethanol but at gas-phase geometry. The UV-Vis spectra were simulated through the fifty-root TD-B3LYP vertical excitation energy calculations by summing Gaussian curves (FWHH = 10 nm) whose areas were fitted to the calculated oscillator strengths *f*. In the presence of ethanol, *o*-anisidine was placed in a cavity formed by a set of overlapping spheres in the frameworks of the solvent reaction field and then ethanol was treated implicitly by using polarizable continuum model (PCM)[32]. Frontier molecular orbital analyses were also performed to determine the nature of electronic transitions. These analyses were also extended to the calculation of some global molecular characteristics.

Charge distribution analyses were performed at both B3LYP/6-31G* and B3LYP/6-311++G** levels. Mulliken, electrostatic potential (ESP), and natural bond orbital (NBO) analyses were used in these atomic charge calculations. Molecular electrostatic potential plots were also obtained for determining nucleophilic and electrophilic regions of *o*-anisidine.

The B3LYP/6-311++G** geometries were subjected to the calculations of the isotropic NMR shielding constant with the Gauge Including Atomic Orbital (GIAO) method at again B3LYP/6-311++G** level. The isotropic ^{13}C and ^{1}H NMR chemical shifts were then obtained by subtracting the shielding constants of *o*-anisidine from those of tetramethylsilane (TMS) calculated at the same computational level (184.07 ppm for C and 31.97 ppm for H). The calculated chemical shifts are generally scaled for correlating them with experiments easier[33-38]. The necessity for the scaling of the chemical shifts arises from the fact that, although the calculations are carried out on single isolated molecules, the recorded NMR spectra are quite sensitive to the environment of the molecules (solvent used or packing in solid state). To assess the effect of geometry on the chemical shifts, the B3LYP/6-311++G** shielding constant calculations were also performed at the B3LYP/6-31G* geometries. The calculated chemical shifts were expressed in this case relative to calculated shielding constants of TMS at the same computational level (183.51 ppm for C and 31.89 ppm for H).

Results and discussion

Molecular geometry

The molecular structures of *o*-anisidine were obtained with geometry optimizations at the B3LYP/6-31G* and B3LYP/6-311++G** levels. Two stable conformers of *o*-anisidine (Conf1 and Conf2; see Figure 1) were located arising from pyramidalized geometry of the amino group. The pyramidalized geometry of the amino group is due to a balance between opposing forces: the stability gained by the molecule as a whole arising from p–π conjugation of the nitrogen lone pair with the aromatic system versus that gained by the amine using highly directed sp^3 orbitals for bond formation [8,9]. This asymmetric interaction between the amino group and the aromatic ring produces a small displacement of the nitrogen atom from the benzene plane.

The C1–N bond orients in Figure 1 outside and inside of the page plane in Conf1 and Conf2 of *o*-anisidine, respectively. Therefore, amino hydrogen atoms orient at the opposite directions, i.e., inside and outside the page plane in Conf1 and Conf2, respectively. Only the rotamer due to methyl orientation with a dihedral angle C2–O–C–H_{met} of ~180° is stable with vibrational frequencies that are all real. The other rotamers due to the methyl orientation have at least one imaginary frequency, and thus are not stable.

The Conf1 and Conf2 of *o*-anisidine are virtually degenerate, with slight preference to Conf2 (0.005 kcal/mol). The transition structure that connects Conf1 and Conf2 has planar amino group and lies just 0.74 kcal/mol above these conformers.These energetic data suggest that Conf1 and Conf2 of *o*-anisidine coexist at the room temperature as a mixture and are interconverted to each other fast.

The key geometry parameters (bond lengths, bond angles and torsional angles) of Conf1 and Conf2 obtained at the B3LYP/6-31G* and B3LYP/6-311++G** levels are as given in Table 1 using the atom labeling scheme shown on Figure 1. The Conf1 and Conf2 of *o*-anisidine do not contain any symmetry element other than identity. Thus, they belong to the C_1 point group.

The C1–N bond of *o*-anisidine is out of the ring plane by 1.5° while the angle between the planes of the ring and amino group is calculated as 27° and 25° with 6-31G* and 6-311++G** basis sets, respectively (see the bottom of Table 1). These parameters about the structure of the amino group are very similar to those observed in aniline and its other derivatives [8,9,28]. The most significant geometry parameter differences between the 6-31G* and 6-311++G** geometries are due to amino group torsion angles and amount to 2°.

The aromatic ring of *o*-anisidine is obviously distorted from a regular hexagon (Table 1), analogous to the observations on aniline and its other derivatives [8,9,28]. The C2–O bond of *o*-anisidine lies almost in the ring plane (see the bottom of Table 1). The investigated molecular characteristics and spectra of this study have been found to be unaffected from the out of plane direction of the C1–N bond of *o*-anisidine. Therefore, in the following, conformer-specific discussion could not be made. In contrast, for 2-(methylthio) aniline (abbreviated as 2MTA) that contains sulfur in the place of oxygen of *o*-anisidine, the C2–S bond is out of the ring plane by 1–2° [28]. Therefore, both C1–N and C2–S bonds of 2MTA have two orientations, resulting in four conformers. The calculated molecular characteristics of 2MTA conformers that have the C1–N and C2–S bonds at the same and opposite sides of the ring plane vary, while experimental spectra have signals from all these energetically close 2MTA conformers [28].

Vibrational spectra

Several experimental IR and Raman spectra of *o*-anisidine (being liquid) recorded under different experimental settings were taken from spectral databases (gas phase IR [15]; IR in CCl4 [16]; liquid film IR [16]; Raman in a Pyrex tube [17]). They are shown on Figure 2 and 3 together with the calculated IR and Raman spectra plotted using the scaled frequencies. The experimental and calculated vibrational characteristics of *o*-anisidine (frequencies, Raman scattering activities, IR/Raman intensities, assignments of the modes in terms of the percent PED of internal coordinates, and the correlation of the *o*-anisidine modes with benzene modes) are as given in Table 2.

Even after scaling, the calculated frequencies above 2800 cm^{-1} deviate significantly from the experimental frequencies. When compared with the gas-phase IR spectrum, standard error S and

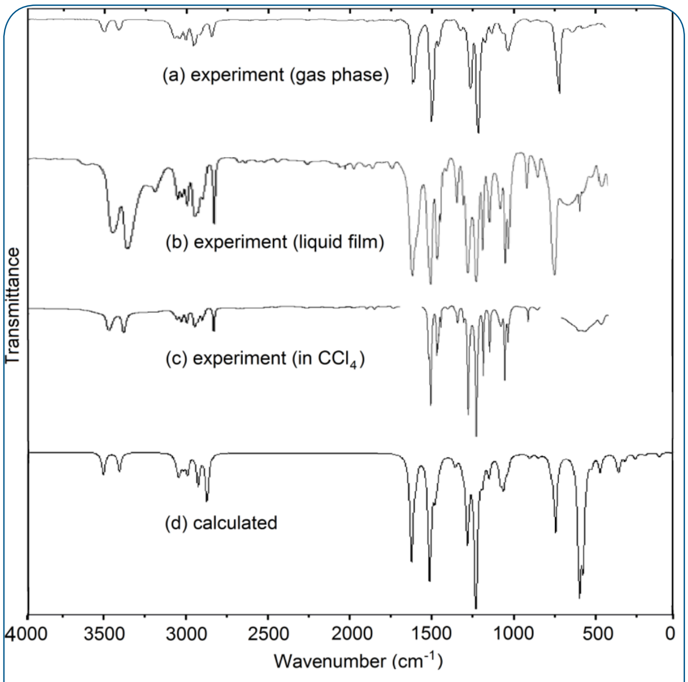

Figure 2: Experimental and simulated IR spectra of *o*-anisidine

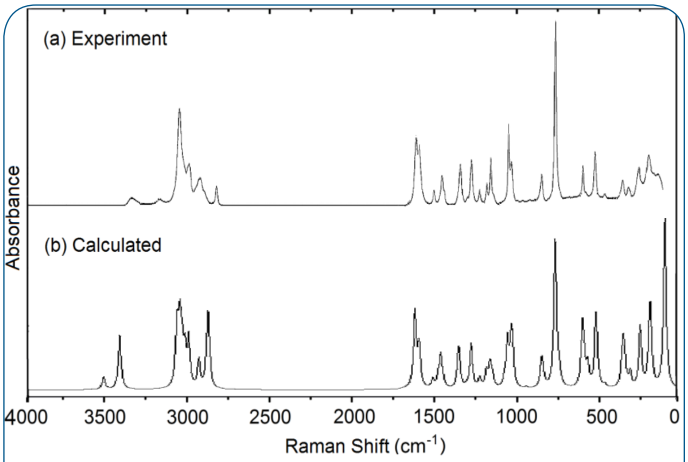

Figure 3: Experimental and simulated Raman spectra of *o*-anisidine

Citation: Ahmet Altun and Kubra Fevzioglu (2016) Structure and Spectroscopy of o-anisidine Investigated by Density Functional Theory in Comparison with Experiments. JApl Theol 1(1): 1-13.

Table 1: Selected B3LYP/6-31G* and B3LYP/6-311++G** geometry parameters of *o*-anisidine

Parameters	**B3LYP/6-31G***		**B3LYP/6-311++G****	
	Conf1	**Conf2**	**Conf1**	**Conf2**
Interatomic distance (Å)				
C1-C2	1.416	1.415	1.413	1.413
C2-C3	1.392	1.392	1.390	1.390
C3-C4	1.401	1.401	1.399	1.399
C4-C5	1.391	1.391	1.389	1.389
C5-C6	1.398	1.398	1.395	1.395
C1-C6	1.398	1.398	1.396	1.396
C2-O	1.376	1.376	1.374	1.374
C7-O	1.416	1.416	1.420	1.420
C1-N	1.397	1.397	1.394	1.394
N-H1	1.012	1.012	1.010	1.010
N-H2	1.012	1.012	1.009	1.009
C-H (ring)[a]	1.086	1.086	1.084	1.084
C-H (meth.)[a]	1.096	1.096	1.093	1.093
Bond angle (degree)				
C1-C2-C3	120.6	120.6	120.6	120.6
C2-C3-C4	120.1	120.1	120.2	120.2
C3-C4-C5	119.8	119.8	119.7	119.7
C4-C5-C6	120.1	120.1	120.1	120.1
C5-C6-C1	121.0	121.0	121.1	121.1
C6-C1-C2	118.3	118.3	118.3	118.3
N-C1-C2	119.2	119.2	119.3	119.3
N-C1-C6	122.4	122.4	122.3	122.4
C1-N-H_{N1}	113.5	113.5	114.7	114.7
C1-N-H_{N2}	114.5	114.5	115.7	115.7
H-N-H	112.3	112.3	113.5	113.5
H_{met}-C-H_{met}[a]	109.3	109.3	109.4	109.4
C2-O-C7	118.1	118.1	118.5	118.5
C1-C2-O	114.2	114.2	114.4	114.4
C3-C2-O	125.1	125.1	125.0	125.0
Torsional angle (degree)				
H_{N2}-N-C1-C2	153.0	-153.0	154.9	-155.3
H_{N1}-N-C1-C2	22.3	-22.3	19.9	-20.1
H_{N2}-N-C1-C6	-29.6	29.6	-27.7	27.4
H_{N1}-N-C1-C6	-160.4	160.4	-162.8	162.6
O-C2-C3-C4	-179.3	179.3	179.3	179.4
C6-C1-C2-O	179.1	-179.1	179.2	-179.3
C1-C2-O-C7	-179.4	179.5	-179.9	-179.8
C3-C2-O-C7	-0.005	0.049	-0.4	0.6
N-C1-H_{N1}-H_{N2}	-27.1	27.0	-24.7	24.6
C1-C6-C2-N	1.5	-1.5	1.5	-1.5
C2-C1-C3-O	-0.3	0.3	-0.3	0.2

[a] Averaged values

Citation: Ahmet Altun and Kubra Fevzioglu (2016) Structure and Spectroscopy of o-anisidine Investigated by Density Functional Theory in Comparison with Experiments. JApl Theol 1(1): 1-13.

Table 2: Calculated B3LYP/6-311++G** vibrational frequencies (in cm^{-1}), IR intensities, Raman scattering activities, Raman intensities, and normal mode descriptions of *o*-anisidine together with its experimental vibrational spectral characteristics

No[a]		Experimental[b]								Calculated					PED (%)
		IR (gas phase)[c]		IR (liquid film)[d]		IR (in CCl4)[d]		Raman[e]		Bare	Scal	I_{IR}	S_{Ra}	I_{Ra}	
1		3501	m	3460	s	3787	m			3674	3542	27.41	47.89	15.91	100 vNH$_2$ (asym.)
2		3412	m	3370	s	3396	m	3355	w	3571	3442	23.03	189.71	69.36	100 vNH$_2$ (sym.)
3	2	3191	w	3198	w			3183	w	3204	3088	7.60	145.26	74.56	88 vCH
4	20b	3073	m	3060	m	3063	w	3066	s	3188	3073	21.21	139.23	72.53	91 vCH
5	7b	3044	m	3047	m	3037	w			3173	3059	7.24	81.11	42.83	91 vCH
6	13			3033	m					3155	3042	11.82	79.19	42.51	92 vCH
7		3006	m	3002	m	3002	w	2999	m	3130	3018	22.12	110.64	60.78	97 vCH$_3$ (asym.)
8		2959	m	2956	m	2955	w			3062	2952	37.57	60.53	35.43	100 vCH$_3$ (asym.)
9		2921	m	2908	m	2908	w	2936	m	3004	2896	57.69	159.83	98.67	98 vCH$_3$ (sym)
10		1625	s	1615	s			1610	s	1654	1623	126.11	42.43	95.59	54 βNH$_2$ (sciss.); 24 vCC; 18 βCH
11	8b	1619	s							1632	1601	13.10	6.34	14.65	77 βCCC; 17 βNH$_2$ (rock.)
12	8a							1596	s	1625	1594	9.78	18.57	43.23	51 vCC; 47 βNH$_2$ (sciss.)
13	19a	1512	vs	1505	s	1506	s	1509	w	1539	1510	147.23	4.39	11.27	47 βCH; 27 βCCC; 16 βCH$_3$
14		1470	m	1466	s	1468	m			1506	1478	36.12	4.43	11.81	81 βCH$_3$ (asym.); 15 vCC
15	19b			1460	m	1461	m	1458	m	1491	1463	9.76	2.25	6.10	35 βCH; 38 βCH$_3$ (sym.); 20 vCC
16						1454	m			1490	1462	8.70	12.84	34.88	71 βCH$_3$ (asym.); 16 βCH
17				1442	m	1442	m			1474	1446	3.21	2.36	6.54	64 βCH$_3$ (sym.); 21 βCH
18	3	1332	m	1341	m	1339	w	1340	m	1377	1351	11.39	17.18	53.41	33 βCH; 32 vCC; 23 βNH$_2$ (rock.)
19	14			1303	m	1304	w			1330	1305	10.08	0.62	2.03	60 βCH; 17 vCC; 11 βNH$_2$ (rock.); 10 βCH$_3$
19	14			1303	m	1304	w			1330	1305	10.08	0.62	2.03	60 βCH; 17 vCC; 11 βNH$_2$ (rock.); 10 βCH$_3$
20	20a	1274	s	1275	s	1275	s	1278	m	1300	1275	99.45	16.50	56.46	41 βCH; 26 βCCC; 27 vCN; 12 βCH$_3$ (sym.)
21		1227	vs	1226	s	1225	vs	1224	w	1246	1222	198.32	3.58	13.14	46 v(CO+OCH$_3$); 29 βCH; 24 βCCC
22		1186	m	1182	s	1183	s	1190	w	1203	1180	23.85	5.08	19.69	64 βCH$_3$ (asym.); 15 βCH; 10 βNH$_2$ (rock.)
23	9a							1157	m	1182	1160	0.37	7.01	27.93	86 βCH
24		1145	m	1141	m	1142	m			1169	1147	0.74	2.61	10.58	89 βCH$_3$ (asym.); 10 ϒCOC
25	7a									1163	1141	22.03	1.54	6.29	54 βCH; 21 βNH$_2$ (rock.); 14 βCH$_3$
26		1079	m	1074	m	1072	m			1090	1070	27.85	2.01	9.09	38 βNH$_2$ (rock.); 32 βCH; 15 vCC; 14 vOCH$_3$
27	18b	1046	m	1045	s	1048	s	1043	s	1069	1049	34.71	12.78	59.62	51 βCH; 20βCCC; 23 vOCH$_3$

No[a]		Experimental[b]								Calculated					PED (%)
		IR (gas phase)[c]		IR (liquid film)[d]		IR (in CCl4)[d]		Raman[e]		Bare	Scal	I_{IR}	S_{Ra}	I_{Ra}	
28	18a			1025	s	1029	s	1031	s	1045	1025	15.84	15.33	74.04	57 βCCC; 25 βNH$_2$ (twist.); 18 vOCH$_3$ (sym.)
29	17a	906	w	911	m	906	w			954	936	0.07	0.39	2.17	86 ϒCH; 14 ϒCCC
30	5									906	888	4.89	0.08	0.45	79 ϒCH; 17 ϒCCC
31	12	835	w	843	m	841	w	840	m	852	836	3.59	5.81	38.01	66 βCCC; 23 ϒNH$_2$ (wag.)
32	17b									840	824	0.64	0.54	3.59	69 ϒCH; 21 ϒCCC
33	6b							757	vs	768	754	14.69	24.85	189.14	60 βCCC; 26 βOCH$_3$; 13 βNH$_2$ (rock.)
34	10a	734	s	742	s					747	733	1.19	0.43	3.38	53 ϒCH; 36 ϒCCC
35	4									742	728	91.89	1.24	9.90	80 ϒCH; 14 ϒCCC
36	6a	593	w	586	m	586	m	589	m	599	587	5.22	6.90	75.26	60 βCCC; 19 ϒNH$_2$ (wag.); 16 βCH$_3$
37										588	577	152.21	2.18	24.42	48 ϒNH$_2$ (wag.); 46 ϒCCC
38	16b									565	554	107.30	2.13	25.27	51 ϒCCC; 42 ϒNH$_2$ (wag.)
39	15							515	m	514	504	4.38	5.17	70.33	38 βCN; 36 βCO; 26 βCCC
40	9b									510	500	5.97	2.14	29.46	43 βCCC; 26 ϒNH$_2$ (wag.); 35 βCOC
41	1			450		453	w	457	w	456	448	20.21	0.26	4.18	65 ϒCCC; 19 ϒNH$_2$ (wag.); 10 βCOC
42								347	w	352	346	20.68	1.12	26.85	46 ϒNH$_2$ (twist.); 24 ϒCCC; 27 βCH$_3$
43										339	333	6.34	2.33	59.14	55 ϒNH$_2$ (twist.); 21 ϒOCH$_3$ (tors.); 24 ϒCCC
44	16a							308	w	300	295	6.25	0.59	18.23	46 ϒCCC; 39 ϒCOC; 24 ϒCN
45								242	m	235	230	2.86	0.77	35.26	46 ϒCH$_3$ (tors.); 29 ϒCCC; 19 βCN
46	10b									232	228	4.25	0.89	41.51	48 ϒCH$_3$ (tors.); 28 ϒCCC; 16 ϒCN
47	11							188	m	173	170	2.74	1.40	106.73	41 ϒCO;40 ϒCCC; 20 ϒCN
48										80	79	5.00	0.72	215.90	59 ϒOCH$_3$; 39 ϒCCCC (aniline tors.)

[a] The second entry labels the modes according to the Varsanyi's convention.

[b] s, strong; vs, very strong; m, medium; w, weak; vw, very weak; sh, shoulder.

[c] Taken from Ref. [15].

[d] Taken from Ref. [16]. The mixing parts of the IR spectra of *o*-anisidine and CCl_4 are not reported.

[e] Taken from Ref. [17].

mean absolute error *MAE* in the scaled frequencies are 45 and 30 cm^{-1}, respectively. The *S* and *MAE* are 54 and 33 cm^{-1} compared with the liquid film IR spectrum. The R^2 value of the correlations in this range is 1.0. Therefore, the largeness of the error in the scaled frequencies doe not arise from the use of scaling factor derived on benzene. The differences in the experimental frequencies of this range are mainly due to NH stretchings that are expected to be strongly environment-dependent and anharmonic. The calculated frequencies of the NH stretchings agree better with the gas-phase experimental IR frequencies than those observed in the other experimental settings since the calculations are also performed in the gas phase.

The modes with frequencies below 2800 cm^{-1} are not much affected from the experimental settings. Their frequencies are almost the same in the presently available experimental spectra. The *S* and *MAE* for the calculated frequencies of this range after scaling are just 9 and 6 cm^{-1}, respectively. Therefore, the scaling factor of the frequencies of this range derived on benzene is transferrable to other related molecules.

The 30 benzene-like normal modes of *o*-anisidine are labeled (second entry in Table 2) with the convention of Varsanyi and Szoke adapted from the Wilson notation for benzene [39,40]. This allows investigating the substitutional effects on the benzene modes. All benzene modes with the frequencies below 1650 cm^{-1} couple significantly with the amino and methoxy vibrations. This causes significant shifts in the frequencies of some modes, some of which yield order changes. For example, compared with the vibrational modes of 2MTA [28], the orderings of modes 8a and 8b, 12 and 17b, 15 and 10b, and 9b and 1 are exchanged while the frequency of mode 6b upshifts significantly. Such shifts are more significant compared with the *p*-methylaniline (pMA) mode frequencies [8]. The frequencies of the methyl group vibrations of *o*-anisidine (Table 2) are very similar to those in other aniline derivatives [41-44].

The NH$_2$ scissoring and rocking frequencies of *o*-anisidine are nearly the same as those observed in pure aniline and substituted anilines like pMA and 2MTA [8,28]. They are calculated respectively at 1623 and 1069 cm^{-1}, consistent with the experimental data. The strong vibrational band at around 1270 cm^{-1} (calculated at 1275 cm^{-1} for *o*-anisidine) is known as the C-NH$_2$ stretching band in aniline and related compounds [24,34] and couples strongly with the ring modes.

The NH$_2$ wagging (calc. 577 cm^{-1}) and twisting (Ra. 347 cm^{-1}) vibrations are generally weak and thus difficult to locate on the experimental spectra. However, computations show that the frequencies of these vibrations are affected strongly from the neighboring ring substituents [8,28].

The overall intensity patterns of the calculated and experimental spectra are in general quite consistent to each other. However, as a result of the interaction of *o*-anisidine with its environment, the NH and CH stretching bands that lie above 2800cm^{-1} have intensities larger in the experimental IR spectra recorded as liquid film and in CCl$_4$ than in the experimental gas phase and calculated IR spectra. For the same reason, the shapes of the bands that couple with NH$_2$ wagging in the 550-600 cm^{-1} range vary at different experimental conditions.

UV-Vis electronic absorption spectra

The calculated electronic absorption spectra of *o*-anisidine in both gas phase and in ethanol at the TD-B3LYP/6-311++G** level using the B3LYP/6-311++G** geometries were plotted using the λ vertical excitation wavelengths (nm) and the *f* oscillator strengths (Figure 4). The experimental [18] solution-phase UV spectrum of *o*-anisidine recorded in the 210-320 nm range (Figure 4) finds two bands at 236 nm (logε = 3.89) and 286 nm (logε = 3.40). These bands were calculated at 238 and 267 nm, respectively. Therefore, while the wavelength of the experimental band at 236 nm was reproduced perfectly, that of the experimental band at 286 nm is estimated smaller only by around 20 nm. The intensity patterns of these two bands in the calculations and experiment are also consistent to each other. Therefore, the analyses of the electronic absorption spectra of *o*-anisidine at the present computational level are quite promising.

The calculations find four absorption bands for *o*-anisidine above 150 nm that are labeled as A, B, C, and D (Figure 4). While the bands A and C are due to mainly two transitions (a$_1$ and a$_2$ for the band A; c$_1$ and c$_2$ for the band C), the bands B and D can be both assigned to a unique transition labeled b and d (Fig. 4). While the energy ordering of the occupied orbitals of *o*-anisidine in the gas phase [i.e., highest occupied molecular orbital (HOMO) to HOMO−4] is not affected from the introduction of ethanol solution, this causes reordering of the unoccupied orbitals (Figure5). For example, the lowest unoccupied molecular orbital (LUMO), LUMO+1, LUMO+2, LUMO+3, and LUMO+4 in the gas phase structure correspond to LUMO+1, LUMO, LUMO+5, LUMO+4, and LUMO+2 of the structure in ethanol, respectively. The involvement of the unoccupied orbitals in the main

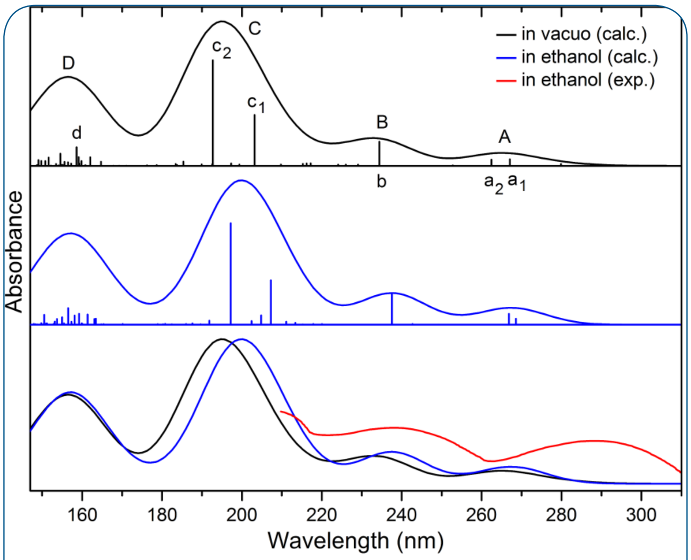

Figure 4: Calculated UV-Vis electronic absorption spectra of *o*-anisidine in both gas phase and ethanol, and their comparisons with the experimental spectrum

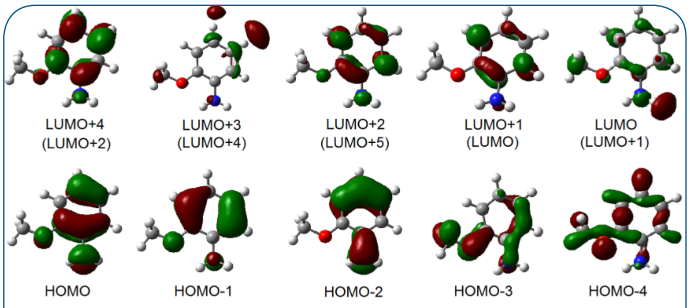

Figure 5: Key frontier molecular orbitals of *o*-anisidine in both gas phase (out of parenthesis) and ethanol (in parenthesis)

transitions of the bands A–D (i.e., a_1, a_2, b, c_1, c_2, and d) varies also going from gas phase to solution structure. Such differences shift all electronic bands slightly to higher wavelengths moving *o*-anisidine from gas phase to ethanol (Figure 4 and Table 3).

We have assigned the main electronic transitions in the UV-Vis spectrum of *o*-anisidine (Table 3) in terms of the frontier molecular orbitals (Figure5). The frontier molecular orbital analyses are also useful in estimating several molecular characteristics like chemical reactivity, kinetic stability, and site of electrophilic attack [45-48]. According to Koopman's theorem [49], the HOMO and LUMO energies are the negative ionization potential I and the negative electron affinity A, respectively.

$$E_{HOMO} = -I \ ; \ E_{LUMO} = -A$$

The relation of I and A with some other global molecular characteristics like electronegativity χ, chemical hardness η, chemical potential μ, and electrophilicity index ω are as follows [49-53]:

$$\chi = \frac{I+A}{2} ; \eta = \frac{I-A}{2} ; \mu = -\chi ; \omega = \frac{\mu^2}{2\eta}$$

Therefore, when the HOMO-LUMO energy gap ΔE is widened, the hardness of the molecule increases while its reactivity decreases [51-54]. The calculated global molecular characteristics of *o*-anisidine obtained using the above relations at the B3LYP/6-311++G** level are given in Table 4 for both gas-phase and ethanol structures. These data suggest that *o*-anisidine becomes slightly more stable and slightly less reactive in the solution, owing to its increased ionization potential and reduced electron affinity.

Table 3: The λ vertical excitation wavelengths (nm) and *f* oscillator strengths calculated at TD-B3LYP/6-311++G** level for the most intense electronic transitions in each band of the UV-Vis spectrum of *o*-anisidine in both gas phase and ethanol

Band	Transition	λ (nm)	*f*	Assignment[a,b]
In gas phase				
A	a_1	267	0.03	HOMO → LUMO+1 (82%)
	a_2	262	0.03	HOMO → LUMO+2 (79%)
B	b	234	0.11	HOMO → LUMO+4 (67%)
				HOMO–1 → LUMO+1 (10%)
C	c_1	203	0.24	HOMO–1 → LUMO+2 (29%)
				HOMO–1 → LUMO+1 (18%)
				HOMO–1 → LUMO+4 (15%)
	c_2	193	0.50	HOMO–1 → LUMO+4 (53%)
D	d	155	0.06	HOMO–3 → LUMO+1 (41%)
				HOMO–4 → LUMO+1 (12%)
				HOMO–4 → LUMO (10%)
In ethanol				
A[c]	a_1	269	0.03	HOMO → LUMO+1 (47%)
				HOMO → LUMO (40%)
	a_2	267	0.06	HOMO → LUMO (51%)
				HOMO → LUMO+1 (33%)
B[d]	b	238	0.17	HOMO → LUMO+4 (70%)
				HOMO–1 → LUMO+1 (11%)
C	c_1	207	0.25	HOMO–1 → LUMO+1 (48%)
				HOMO–1 → LUMO+4 (12%)
	c_2	197	0.58	HOMO–1 → LUMO+4 (58%)
				HOMO–1 → LUMO+1 (12%)
D	d	157	0.09	HOMO–3 → LUMO+1 (43%)
				HOMO–4 → LUMO+1 (24%)

[a] The transitions that contribute less than 10% are not shown.

[b] To allow direct comparisons for the orbital types involved in the transitions of gas-phase and ethanol spectra, the orbital labeling of the gas phase structure was used. For example, the LUMO orbital of the gas-phase structure is the LUMO+1 orbital of the structure in ethanol. Instead of LUMO+1 of the structure in ethanol, its relevant orbital in the gas phase structure, i.e., LUMO, was written.

[c] Experimental values: λ_{max} =286 nm; logε = 3.40

[d] Experimental values: λ_{max} = 236 nm; logε = 3.89

Table 4: The calculated global molecular characteristics (eV) of *o*-anisidine at the B3LYP/6-311++G** level in gas phase and ethanol

Parameters	In vacuo	In ethanol
E_{HOMO}	-5.44	-5.55
E_{LUMO}	-0.28	-0.22
ΔE	-5.16	-5.33
I	5.44	5.55
A	0.28	0.22
χ	2.86	2.89
η	2.58	2.67
μ	-2.86	-2.89
ω	1.59	1.56

Charge distribution and molecular electrostatic potential analyses

Charge distribution analyses have been performed with B3LYP functional by using both the small 6-31G* and the larger 6-311++G** basis sets and by applying Mulliken, ESP, and the most sophisticated NBO schemes (Figure6). The average of the already-similar charges for the ring hydrogens (H_{ring}), hydrogens bonded to the nitrogen atom (H_N), and the methyl hydrogens were used in plotting Figure 6.

All calculated charges are reasonably close to each other except the Mulliken charges calculated with the larger 6-311++G** basis set for the ring atoms. Mulliken/6-311++G** charges of the ring atoms differ from the other calculated charges not only in the amount significantly but also in the sign. Therefore, one must suspect about the quality of the Mulliken charges when more diffuse and polarization functions are added to the 6-31G* basis set. Actually, the success of the Mulliken scheme with the 6-31G* basis set is not surprising since its parameterization is already based on this basis set [55].

Although ESP charge scheme is more sophisticated than the Mulliken charge scheme, it may also be problematic for electronegative and their neighboring atoms, where the overlap between two orbitals are not partitioned equally [54]. Such kinds of problems in the ESP scheme are not much effective on *o*-anisidine. The most striking difference in the ESP and the most sophisticated NBO charges is the charge of the oxygen atom, being ~0.55*e* in the NBO and Mulliken analyses and ~0.25*e* in the ESP analysis. However, the ESP analysis finds also the oxygen atom as one of the most electronegative atom.

The present calculations suggest the most negative atoms as nitrogen and then oxygen. All hydrogen atoms have positive charges; the most is being on the hydrogens bonded to the nitrogen atom. The ring carbons where the substitution occurs have positive charges while the other carbons have negative charges.

Molecular electrostatic potential (MESP) can be determined experimentally through diffraction methods [55] or be calculated from the electron density, which is obtained in the present case from DFT by applying the following formula [56]

$$V(\vec{r}) = \sum \frac{Z_A}{\vec{R}_A - \vec{r}} \int \frac{\rho(\vec{r}\,')}{|\vec{r}\,' - \vec{r}|} d\rho'$$

where Z_A is the charge on nucleus A that has the position vector $\vec{R}_A$ and ρ is the electron density at the position $\vec{r}\,'$.

The plot of MESP of *o*-anisidine calculated at the B3LYP/6-311++G** is shown in Figure7. In this plot, going from violet to red, electrostatic potential decreases. Therefore, the violet and red regions correspond to positive and negative electrostatic potentials, respectively. The hydrogen atoms reflect positive potential, and thus are the sites of electrophilic attack while the nitrogen and oxygen atoms bear the most electronegative region, and thus have high nucleophilic activity.

Nuclear magnetic resonance spectra

The results of the present GIAO-B3LYP/6-311++G** level chemical shift calculations at both B3LYP/6-31G* and B3LYP/6-311++G** geometries were used in assigning the signals in the experimental [16] ^{13}C and ^{1}H NMR spectra of *o*-anisidine recorded in $CDCl_3$ (Table 5) to specific carbons and protons. GIAO-B3LYP/6-311++G** level chemical shift calculations have been already shown to be quite accurate at the B3LYP/6-31G* geometries of several molecules [33-38,57]. The previous GIAO-B3LYP/6-311++G** level chemical shift calculations were mostly performed at B3LYP/6-31G* geometries [33-38,57]. In this study, we also assess the quality of the B3LYP/6-311++G** geometries in reproducing experimental chemical shift values.

The assignments of the NMR signals of *o*-anisidine are as given in Table 5. Although the calculated ^{1}H NMR chemical shifts are very close to the calculated shifts at both geometries, the ^{13}C NMR chemical shifts are overestimated. This arises mainly from the fact that, although the calculations are carried out on single isolated molecules, NMR spectra are quite sensitive to the environment of the molecules, i.e., to the experimental conditions (solvent used or packing in solid state). To relate the experimental and calculated chemical shifts easier, the calculated chemical shifts are generally scaled [33-36,57]. As shown in Figure8, the calculated and experimental chemical shifts correlate very well with R^2 of ~1.0. The correlation equations between the experimental and

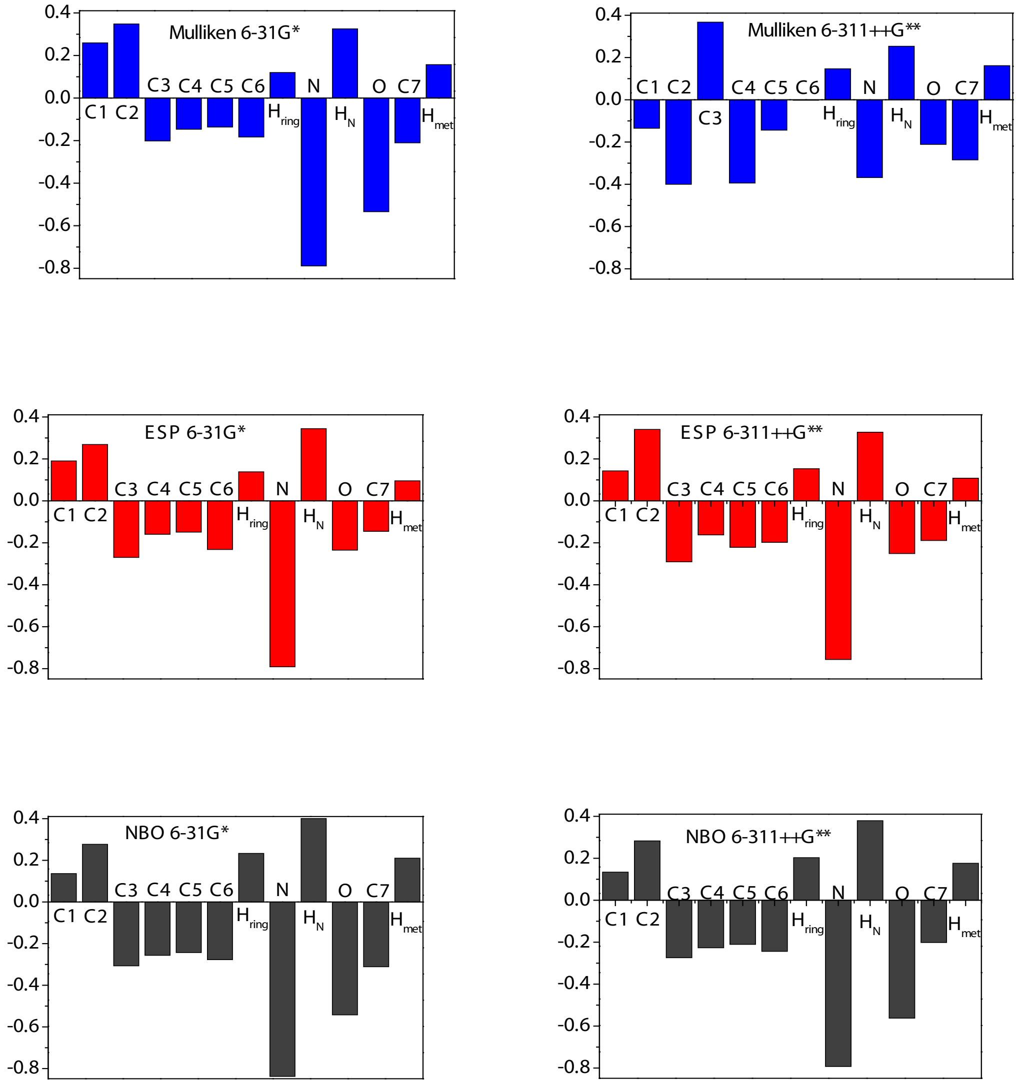

Figure 6: B3LYP charges on each atom of o-anisidine calculated with the 6-31G* (left) and 6-311++G** (right) basis sets using Mulliken (top), ESP (middle), and NBO (bottom) schemes

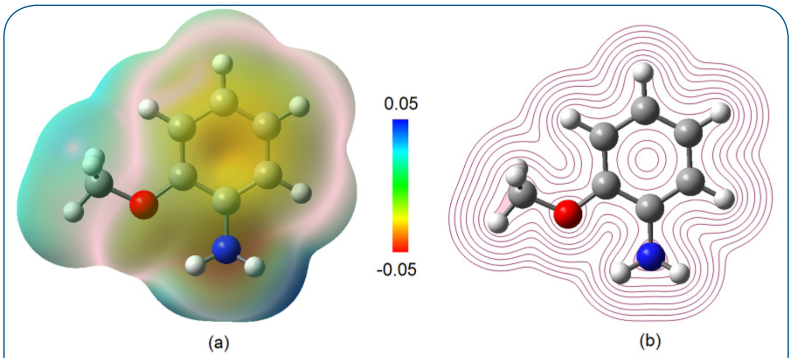

Figure 7: (a) The plot of molecular electrostatic potential of *o*-anisidine obtained from the total B3LYP/6-311++G** SCF electron density, and (b) its projection on the ring plane.

Table 5: The experimental (in $CDCl_3$) and calculated (unscaled and scaled) ^{13}C and ^{1}H GIAO-B3LYP/6-311++G** chemical shifts of *o*-anisidine relative to TMS (in ppm) at both 6-31G* and 6-311++G** geometries

Atom	Experiment[a]	6-31G* Geometry		6-311++G** Geometry	
		Unscaled	Scaled	Unscaled	Scaled
C1	136.37	144.40	137.93	143.83	137.78
C2	147.32	154.26	147.07	153.85	147.15
C3	110.55	112.78	108.65	112.87	108.83
C4	118.30	122.78	117.91	122.54	117.87
C5	121.13	126.85	121.68	126.89	121.94
C6	114.99	119.32	114.71	118.83	114.40
C7	55.30	55.95	56.02	56.38	56.01
H3	6.65	6.59	6.54	6.60	6.54
H4	6.70	6.76	6.70	6.76	6.70
H5	6.76	6.92	6.85	6.94	6.87
H6	6.74	6.79	6.73	6.78	6.72
H_{met}	3.77	3.84	3.92	3.87	3.92
H_N	3.70	3.47	3.57	3.51	3.58

[a] Ref. [16]

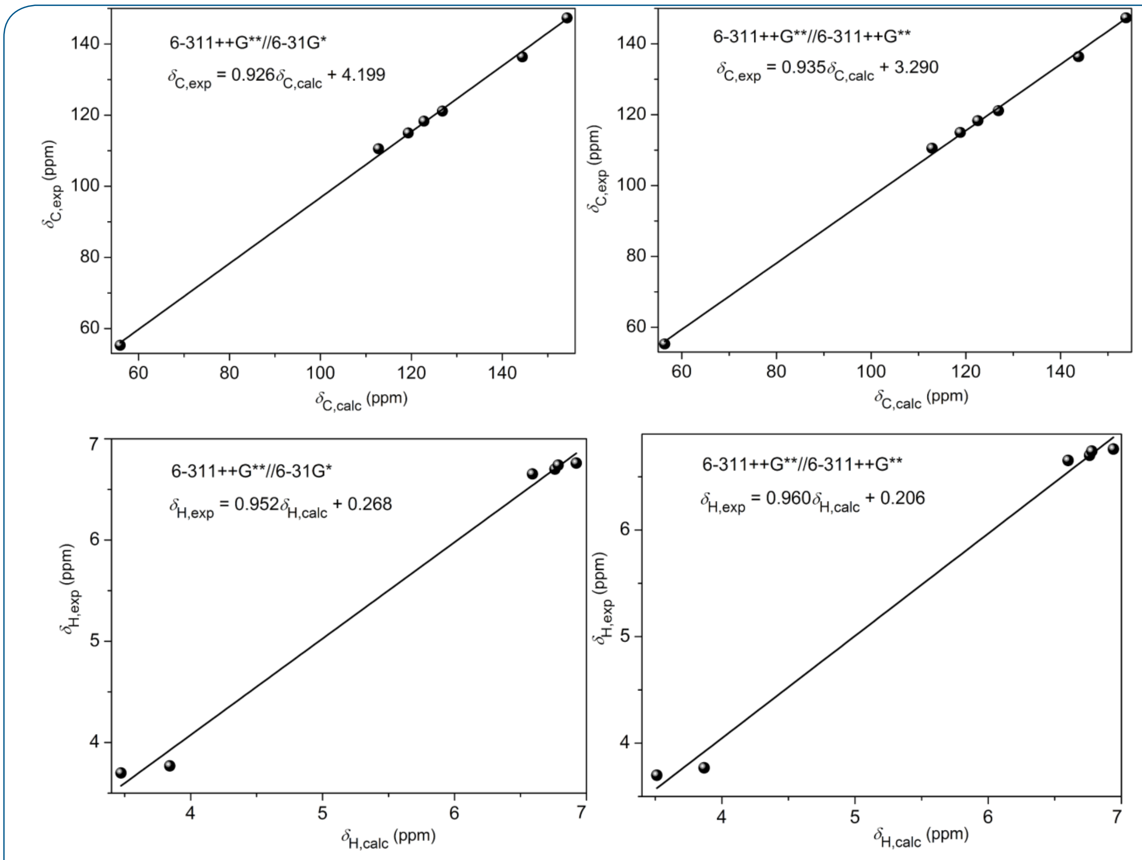

Figure 8: Correlation between the experimental and calculated GIAO-B3LYP/6-311++G** level (at both 6-31G* and 6-311++G** geometries) ^{13}C and ^{1}H chemical shifts of *o*-anisidine relative to TMS (in ppm)

calculated chemical shifts δ (in ppm) are as follows

$$\delta_{C,\exp} = 0.926 \cdot \delta_{C,calc} + 4.199 \quad (S = 1.20;\ MAE = 0.81)$$

$$\delta_{H,\exp} = 0.952 \cdot \delta_{H,calc} + 0.268 \quad (S = 0.12;\ MAE = 0.08)$$

at the 6-31G* geometry, and

$$\delta_{C,\exp} = 0.935 \cdot \delta_{C,calc} + 3.290 \quad (S = 1.15;\ MAE = 0.83)$$

$$\delta_{H,\exp} = 0.960 \cdot \delta_{H,calc} + 0.206 \quad (S = 0.13;\ MAE = 0.09)$$

at the 6-311++G** geometry.

The correlation equations and the associated standard errors

S and the mean absolute deviations *MAE* indicate that the calculated chemical shift values at both geometries are quite similar and predictive.

Conclusions

The conformational stabilities, geometrical structures, vibrational spectra (both IR and Raman), UV-Vis electronic absorption spectra, the frontier molecular orbitals together with the related global molecular characteristics, molecular electrostatic potential map, and NMR spectra (^{13}C and ^{1}H) of *o*-anisidine have been investigated by using the hybrid B3LYP density functional. All of these molecular features have been calculated using the triple-ζ 6-311++G** basis set. However, the effects of basis set on some of these characteristics have been studied by using the double-ζ 6-31G* basis set, as well.

As a result of the pyramidalized structure of the amino group, the C–N bond in *o*-anisidine is out of the ring plane, which results in two conformations (Conf1 and Conf2). These two conformers have almost the same energy. Thus, *o*-anisidine exists actually as a mixture of these two conformers at the room temperature. All the calculated properties in this study for these two conformers are almost identical. Therefore, their experimental distinction from the recorded spectra seems unlikely.

All fundamental vibrational (IR and Raman) bands of *o*-anisidine have been assigned in terms of the present calculations, giving PED of each mode with internal coordinates. The simulated IR and Raman spectra of *o*-anisidine using the scaled computational wavenumbers, and IR/Raman intensities have been found quite consistent with the experimental spectra.

The calculated TD-B3LYP and experimental electronic absorption spectra of *o*-anisidine agree to each other reasonably. Introducing *o*-anisidine with ethanol affects the energy ordering of the unoccupied orbitals and the involving unoccupied orbitals in the most intense electronic transitions. Such effects shift all electronic bands of *o*-anisidine slightly to longer wavelengths. In the solution, ionization potential of *o*-anisidine increases while its electron affinity decreases. Therefore, solution-phase *o*-anisidine is slightly more stable but less reactive.

In comparison with the results of sophisticated ESP and NBO charges, it has been shown that Mulliken charge analysis is erratic with the 6-311++G** basis set but accurate enough with the smaller 6-31G* basis set, which is already used in parameterization of Mulliken analysis. ESP and NBO charge analyses give similar charges with both basis sets. The most negative atoms of *o*-anisidine are found as nitrogen and then oxygen. All hydrogen atoms have positive charges. The largest positive charges are on the hydrogens bonded to the nitrogen atom. The ring carbons with peripheral substituents have positive charges while the rest of the carbons have all negative charges. The plot of molecular electrostatic potential indicates hydrogens as the sites of electrophilic attack, and N and O to have high nucleophilic activity.

The calculated ^{13}C chemical shifts of *o*-anisidine are slightly larger than the experimental ones. However, the high correlations between the experimental and calculated chemical shifts indicate that the errors in the calculations are systematic and be cured with scaling the chemical shifts. This allowed us certain assignments of the ^{13}C and ^{1}H NMR signals in terms of the present calculations. The calculated B3LYP/6-311++G** chemical shifts at the 6-311++G** and 6-31G* geometries agree very well, with very slight variations. Therefore, both geometries are accurate for calculating NMR properties.

The present structural and spectroscopic calculations have been found quite useful on *o*-anisidine in comparison with the available experiments. Therefore, the computational route followed in this study can be extended in studying molecular characteristics of analogous compounds.

Acknowledgments

This work is supported by the Scientific Research Fund of Fatih University under the project numbers of P50011102_Y (1679).

References

1. Vaschetto ME, Retamal BA, Monkman AP. J. Mol. Str. (Theochem). 1999; 468: 209–221.
2. Tzeng WB, Narayanan K, ShiehK C, Tung CC. J. Mol. Str. (Theochem). 1998; 428: 231–240.
3. Santos L, Martínez E, Ballesteros B, SanchezJ. Spectrochim. Acta. 2000; 56A: 1905–1915.
4. Ramon JMH, Gallego AP, Nunez EM, Ramos AF, Lago EMC. J. Mol. Str. (Theochem). 2000; 497: 105–113.
5. Golcuk K, Altun A, Kumru M. Spectrochim. Acta. 2003; 59A: 1841–1847.
6. Golcuk K, Altun A, Kumru M. J. Mol. Str. 2003; 657: 385–393.
7. Ballesteros B, Santos L. Spectrochim. Acta. 2002; 58A: 1069–1081.
8. Altun A, Gölcük K, Kumru M. J. Mol. Str. (Theochem). 2003; 637: 155–169.
9. Altun A, Gölcük K, Kumru M. J. Mol. Str. (Theochem). 2003; 625: 17–24.
10. Akalin E. Akyüz S. J. Mol. Str. 1999; 482–483: 175–181.
11. Stiborová M, Miksanova M, Havlicek V, Schmeiser HH, Frei E. Mutat. Res.-Fund. Mol. M. 2002; 500: 49–66.
12. Stiborova M, Naiman K, Martinkova M, Martinek V, Svobodova M, Schmeiser HH, et al. InterdiscipToxicol. 2009; 2: 24–27.
13. Sivaranjini T, Periandy S, Govindarajan M, Karabacak M, Asiri AM. J. Mol. Str. 2014; 1056–1057: 176–188.
14. Naiman K, Martinkova M, Schmeiser HH, Frei E, Stiborova M. Mutat. Res.-Gen. Tox. En. 2011; 726: 160–168.
15. Chem Spider. A chemical structure database owned by the Royal Society of Chemistry. cited 2015 Jun 6. Available from:http://www.chemspider.com
16. SDBS. Spectral database for organic compounds organized by National Institute of Advanced Industrial Science and Technology (AIST), Japan. cited2015 Jun 6. Available from: http://sdbs.db.aist.go.jp
17. Sigma-Aldrich Handbook / Catolog. cited 2015 Jun 6.Available from: http://www.sigmaaldrich.com/catalog
18. National Institute of Standards and Technology (NIST) Standard Reference Database 69: NIST Chemistry WebBook. cited 2015 Jun 6. Available from: http://webbook.nist.gov/chemistry
19. Becke AD. J. Chem. Phys. 1991; 98: 5648–5652.
20. Lee C, Yang W, Parr RG. Phys. Rev. B. 1988; 37: 785–789.

21. Frisch MJ, Trucks GW, Schlegel HB, Scuseria GE, Robb MA, Cheeseman JR, et al. Gaussian03, Revision C.02. Gaussian, Inc. Wallingford CT. 2004.
22. Dewar MJS, Reynolds CH. J. Comput. Chem. 1986; 7: 140–143.
23. Krishnan R, Binkley JS, Seeger R, PopleJ A. J. Chem. Phys. 1980; 72: 650–654.
24. Raghavachari K, PopleJ A, Replogle ES, Head-GordonM. J. Phys. Chem. 1990; 94: 5579–5586.
25. Hameka HF, Jensen JO. J. Mol. Str. (Theochem). 1996; 362: 325-330.
26. Scott AP, Radom L. J. Phys. Chem. 1996; 100: 16502–16513.
27. Küçük V, Altun A, Kumru M. Spectrochim. Acta. 2012; 85A: 92–98.
28. Altun A, Aghatabay NM. Vib. Spectrosc. 2013; 64: 68–77.
29. Polavarapu PL. J. Phys. Chem. 1990; 94: 8106–8112.
30. Keresztury G. In: Chalmers JM, Griffiths PR, editors. Handbook of Vibrational Spectroscopy. Vol: 1. Wiley; 2002. p. 71.
31. Keresztury G, Holly S, Besenyei G, Varga J, Wang A, Durig JR. Spectrochim. Acta. 1993; 49A: 2007–2026.
32. Tomasi J, Mennucci B, Cances E. J. Mol. Str. (Theochem). 1999; 464: 211–226.
33. Aliev AE, Murias DC, Zhou S. J. Mol. Str. (Theochem). 2009; 893: 1–5.
34. Bally T, Rablen PR. J. Org. Chem. 2011; 76: 4818–4830.
35. Cheeseman JR, Trucks GW, Keith TA, Frisch MJ. J. Chem. Phys. 1996; 104: 5497–5509.
36. Jain R, Bally T, Rablen PR. J. Org. Chem. 2009; 74: 4017–4023.
37. Lodewyk MW, Siebert MR, Tantillo DJ. Chem. Rev. 2012; 112: 1839–1862.
38. Rablen PR, Pearlman SA, Finkbiner J. J. Phys. Chem. A. 1999; 103: 7357–7363.
39. Varsanyi G. Assignments of vibrational spectra of 700 benzene derivatives. New York: Wiley; 1974.
40. Varsanyi G, Szoke S. Vibrational Spectra of Benzene Derivatives. New York: Academic Press; 1969.
41. Golcuk K, Altun A, Somer M, Kumru M. Vib. Spectrosc. 2005; 39: 68–73.
42. Golcuk K, Altun A, Guner S, Kumru M, Aktas B. Spectrochim. Acta. 2004; 60A: 303–309.
43. Altun A, Golcuk K, Kumru M. Vib. Spectrosc. 2003; 33: 63–74.
44. Altun A, Golcuk K, Kumru M. Vib. Spectrosc. 2003; 31: 215–225.
45. Fleming I. Frontier orbitals and organic chemistry reactions. John Wiley & Sons; 1976.
46. Muthu S, Rajamani T, Karabacak M, Asiri AM. Spectrochim. Acta. 2014; 122A: 1–14.
47. Ok S, Altun A, Kasimogullari R, Sen E. J. Chem. Eng. Data. 2013; 58: 3521–3527.
48. Kumru M, Kucuk V, Kocademir M, Alfanda HM, Altun A, Sarı L. Spectrochim. Acta. 2015; 134A: 81–89.
49. Pearson RG. Proc. Natl. Acad. Sci. USA. 1986; 83: 8440–8441.
50. Mebi CA. J. Chem. Sci. 2011; 123: 727–731.
51. Pearson RG. J. Am. Chem. Soc. 1985; 107: 6801–6806.
52. Pearson RG. J. Am. Chem. Soc. 1986; 108: 6109–6114.
53. Pearson RG. J. Am. Chem. Soc. 1988; 110: 7684–7690.
54. Young DC. Computational Chemistry: A Practical Guide for Applying Techniques to Real-World Problems. John Wiley & Sons; 2001.
55. Gholami M, Talebi B, Khalili M. Tetrahedron Lett. 2003; 44: 7681–7685.
56. Murray JS, Sen K. Molecular Electrostatic Potentials: Concepts and Applications. New York: Elsevier; 1996.
57. Altun A, Ok S. J Chem. Eng. Data. 2012; 57: 2619–26.